JUSTC

Letter

http://justc.ustc.edu.cn

Received: December 11, 2022; Accepted: March 20, 2023

Electronic correlation effects on stabilizing a perfect Kagome lattice and ferromagnetic fluctuation in $LaRu_3Si_2$

Yilin Wang ✉

School of Emerging Technology，University of Science and Technology of China，Hefei 230026，China

✉Correspondence: Yilin Wang, E-mail: yilinwang@ustc.edu.cn

Graphical abstract

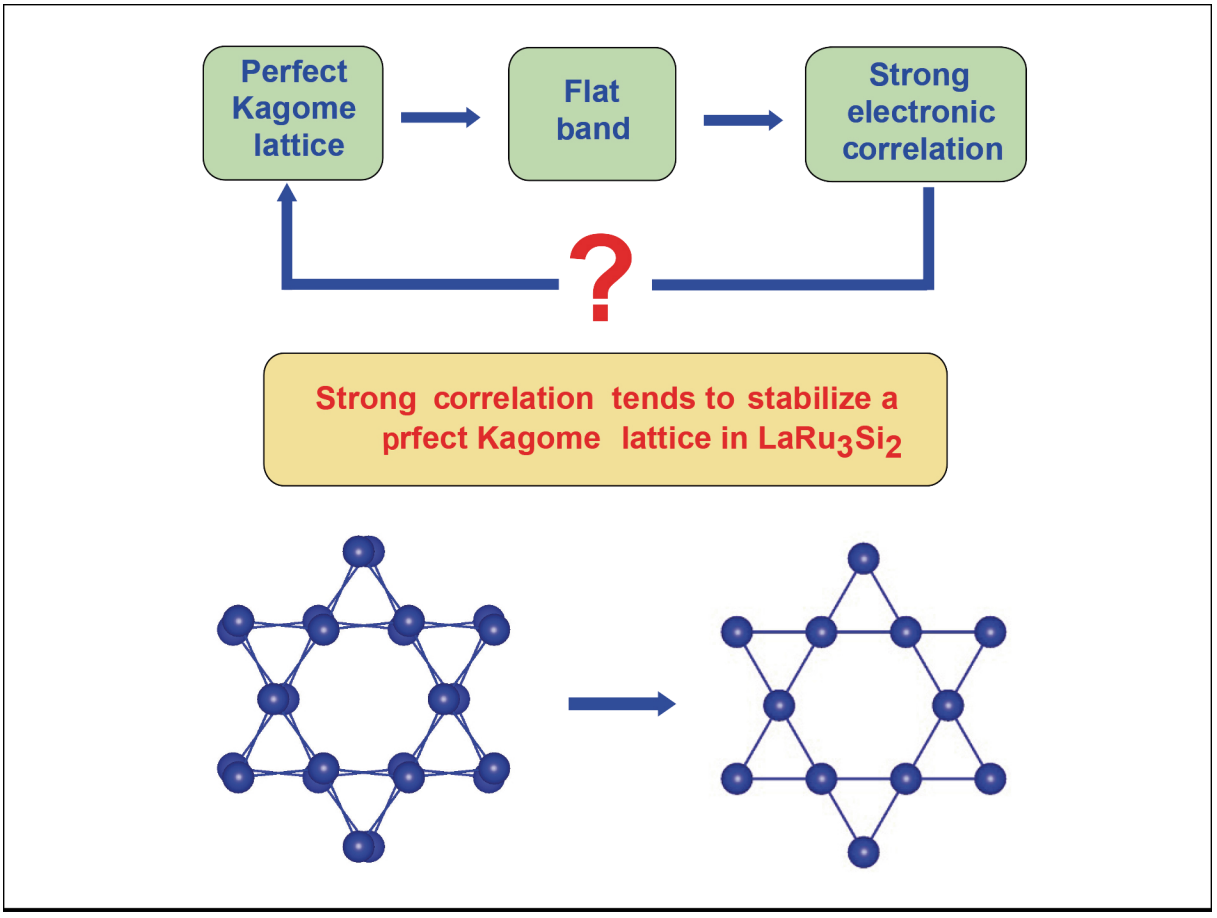

Strong electronic correlations tends to stabilize a perfect Kagome lattice in superconducting Kagome metal $LaRu_3Si_2$.

Public summary

- Electronic correlation effects are found to stabilize a perfect Kagome lattice in superconducting Kagome metal $LaRu_3Si_2$.
- $LaRu_3Si_2$ is found to be on the verge of becoming a perfect Kagome lattice.
- Electronic correlations and ferromagnetic fluctuations are found to be crucial to understand the non-Fermi-liquid behavior and the high superconducting T_c in $LaRu_3Si_2$.

Citation: Wang Y L. Electronic correlation effects on stabilizing a perfect Kagome lattice and ferromagnetic fluctuation in $LaRu_3Si_2$. *JUSTC*, **2023**, 53(7): 0702. DOI: 10.52396/JUSTC-2022-0182

JUSTC

Letter

http://justc.ustc.edu.cn

Received: December 11, 2022; Accepted: March 20, 2023

Electronic correlation effects on stabilizing a perfect Kagome lattice and ferromagnetic fluctuation in $LaRu_3Si_2$

Yilin Wang ✉

School of Emerging Technology, University of Science and Technology of China, Hefei 230026, China

✉Correspondence: Yilin Wang, E-mail: yilinwang@ustc.edu.cn

Cite This: *JUSTC*, **2023**, 53(7): 0702 (5pp)

Read Online

SI Supporting Information

Abstract: A perfect Kagome lattice features flat bands that usually lead to strong electronic correlation effects, but how electronic correlation, in turn, stabilizes a perfect Kagome lattice has rarely been explored. Here, we study this effect in a superconducting ($T_c \sim 7.8$ K) Kagome metal $LaRu_3Si_2$ with a distorted Kagome plane consisting of pure Ru ions, using density functional theory plus U and plus dynamical mean-field theory. We find that increasing electronic correlation can stabilize a perfect Kagome lattice and induce substantial ferromagnetic fluctuations in $LaRu_3Si_2$. By comparing the calculated magnetic susceptibilities to experimental data, $LaRu_3Si_2$ is found to be on the verge of becoming a perfect Kagome lattice. It thus shows moderate but non-negligible electronic correlations and ferromagnetic fluctuations, which are crucial to understand the experimentally observed non-Fermi-liquid behavior and the pretty high superconducting T_c of $LaRu_3Si_2$.

Keywords: electronic correlation; Kagome lattice; $LaRu_3Si_2$; ferromagnetic fluctuation; flat bands

CLC number: O469 **Document code:** A

1 Introduction

A perfect Kagome lattice features flat bands due to the destructive interference of electron hoppings within the geometrically frustrated structure[1–5]. When flat bands are near the Fermi level, they usually induce strong electronic correlation effects, such as unconventional superconductivity[6–11], magnetism[2, 3], topological phases[5], and exotic charge density waves[12, 13]. In recent years, these flat-band-induced correlation effects have been widely studied in Kagome metals, for example, FeSn[14, 15], FeGe[13, 16], Fe_3Sn_2[17–19], CoSn[20–24], and RT_6Ge_6 (R = rare-earth elements, T = Mn, Cr)[25, 26]. But how electronic correlation, in turn, stabilizes a perfect Kagome lattice has rarely been explored. Here, we study this effect in the Kagome metal $LaRu_3Si_2$[27–31] using density functional theory (DFT) plus U[32] and plus dynamical mean-field theory (DMFT)[33–35].

$LaRu_3Si_2$ is a superconductor with a highest $T_c \sim 7.8$ K[27] among the known Kagome superconductors under ambient conditions. It is a paramagnetic metal at high-temperate. Non-Fermi-liquid (NFL) behavior was inferred from transport experiments, indicating substantial electronic correlations from Ru-4*d* orbitals[29]. A recent DFT calculation based on the electron-phonon coupling mechanism yields a $T_c \sim 1.2$ K, much smaller than the experimental value[30], also indicating that other factors, such as electronic correlations and magnetic fluctuations, must be considered to understand its superconductivity.

The perfect Kagome structure of $LaRu_3Si_2$ with space group P6/mmm is shown in Fig. 1a and c. The Kagome layer consists of pure Ru atoms, different from most other Kagome materials in which an anion usually resides in the center of the hexagon of the Kagome structure. Adjacent to the Kagome layer is a layer consisting of a triangular lattice of La and a honeycomb lattice of Si. However, a previous X-ray diffraction study showed that $LaRu_3Si_2$, in reality, crystallizes into a slightly distorted Kagome structure with a doubling of the c-axis and the space group $P6_3/m$[27] (see Fig. 1b and e). Given that only one kind of ion (Ru) is present in the Kagome layer of $LaRu_3Si_2$, it provides an ideal platform for studying its electronic correlation effects on stabilizing a perfect Ru Kagome lattice since it rules out possible crystalline field effects of anion on the stability of the Kagome lattice.

Our calculations find that increasing electronic correlation can stabilize a perfect Kagome lattice and induce substantial ferromagnetic fluctuations in $LaRu_3Si_2$. By comparing the calculated magnetic susceptibilities to experimental data, $LaRu_3Si_2$ is found to be on the verge of the transition from a distorted to a perfect Kagome lattice. It thus shows moderate but non-negligible electronic correlations and ferromagnetic fluctuations, consistent with the experimentally observed NFL behavior[29]. Furthermore, our calculations show that the distorted Kagome structure of $LaRu_3Si_2$ may hold higher symmetry (space group $P6_3/mcm$, see Fig. 1d) than that reported by a previous experiment ($P6_3/m$)[27], which should be further examined by high-resolution crystal structure refinement with high-quality samples.

2 Methods

We perform DFT+U calculations using the VASP package[37, 38], with the exchange-correlation functional of both the local density approximation (LDA) and generalized gradient approximation (GGA)[39]. The energy cutoff of the plane-wave

DOI: 10.52396/JUSTC-2022-0182

JUSTC, **2023**, 53(7): 0702

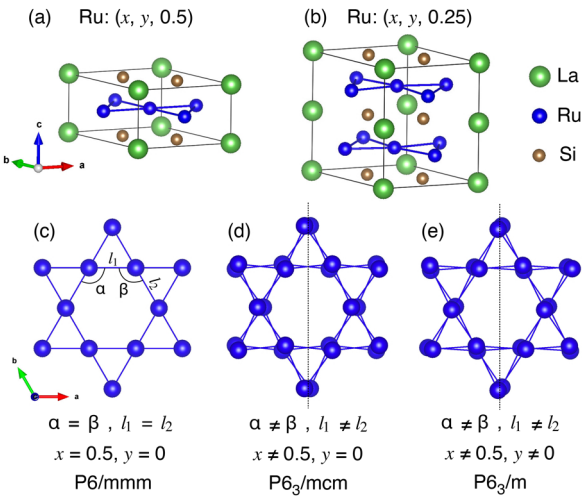

Fig. 1. Three possible crystal structures of $LaRu_3Si_2$ with a Kagome plane consisting of pure Ru atoms. (a), (c) Perfect Kagome structure. (b), (d), and (e) Two possible distorted Kagome structures with a doubling of the c-axis. (c)–(e) Top view of the Kagome planes. The angles α, β and side lengths l_1, l_2 of the hexagon, the fractional coordinates of Ru atoms x, y, and the space group are shown, respectively. The crystal structures are constructed by VESTA[36].

basis is set to 500 eV, and a Γ-centered $21\times21\times21$ k-point grid is used. The internal atomic positions are relaxed in the non-magnetic states until the force of each atom is smaller than 1 meV/Å. The rotationally invariant DFT+U method introduced by Liechtenstein et al.[40] is used, which is parameterized by Hubbard U and Hund's coupling J_H (LDAUTYPE = 1 or 4). It turns out that the spin-orbital coupling (SOC) of Ru would not change the main conclusions, so we only present the non-SOC results in the main text, and an SOC result is presented in Fig. S1. The energies of two magnetic orders, ferromagnetic (FM) and A-type anti-ferromagnetic (AFM) (Fig. S2), are also calculated by GGA+U.

We also perform fully charge self-consistent LDA+DMFT calculations in the paramagnetic states of $LaRu_3Si_2$, using the code EDMFTF developed by Haule et al.[41, 42] based on the WIEN2K package[43]. We choose a wide hybridization energy window from –10 eV to 10 eV with respect to the Fermi level. All 5 Ru-4d orbitals are considered as correlated ones and a local Coulomb interaction Hamiltonian with rotationally invariant form is applied. The local Anderson impurity model is solved by the continuous time quantum Monte Carlo (CTQMC) solver[44]. We use an "exact" double counting scheme invented by Haule[45]. The self-energy on real frequency $\Sigma(\omega)$ is obtained by the analytical continuation method of maximum entropy. We follow the method introduced by Haule et al.[46] to perform structure relaxation in the framework of LDA+DMFT. All the calculations are preformed at $T = 290$ K. Following Ref. [42], we use the Yukawa representation of the screened Coulomb interaction, in which there is a unique relationship between U and J_H. If U is specified, J_H is uniquely determined by a code in EDMFTF[47]. Their values are tabulated in Table S1 and are also used for the DFT+U calculations.

To reveal the role of electronic correlation effects on stabilizing a perfect Kagome lattice in $LaRu_3Si_2$, first, we vary the Hubbard U from 0 to 6 eV in our calculation; second, we perform a comparative study on a hypothetical crystal structure $LaFe_3Si_2$ with the same lattice parameters and initial atomic positions as $LaRu_3Si_2$, since Fe-3d orbitals are expected to show stronger electronic correlations than Ru-4d orbitals. To uncover how the adjacent $LaSi_2$ layers affect the stability of the Ru_3 Kagome layer, we also perform comparative calculations by varying the lattice parameter ratio c/a with the fixed crystal volume from experiment. The experimental lattice parameters are $a = 5.676$ Å, $c = 7.12$ Å, which gives a volume of 198.65 $Å^3$ [27]. A crystal structure with space group $P6_3/m$ and Ru sites at ($x = 0.52$, $y = 0.01$, $z = 0.25$) is constructed as the starting point for relaxation (see Fig. 1b and e). However, all the relaxations converge to the higher symmetry structure with space group $P6_3/mcm$ ($x \neq 0.5$, $y = 0$, $z = 0.25$), where an additional C_2 and mirror symmetry is present (see Fig. 1d). Therefore, we will only discuss the results of space group $P6_3/mcm$ below.

3 Results

Fig. 2a, b, d, and e show the fractional coordinate x of Ru (Fe) relaxed by the LDA+U, GGA+U, and LDA+DMFT methods, for different c/a ratios. For $LaRu_3Si_2$, as U increases, all the methods yield a tendency for x to decrease and approach to the value of a perfect Kagome lattice (0.5). We note that $LaFe_3Si_2$ converges to the perfect Kagome structure even at $U = 0$. Compared to LDA+U, the GGA+U method is expected to describe the correlation effects better, giving a smaller x (dashed curves in Fig. 2a). Fig. 2c and f show the LDA+DMFT calculated orbital-resolved quasi-particle mass-enhancement, $m^\star/m^{\mathrm{DFT}} = 1/Z$, due to the electronic correlation effects, where Z is the quasi-particle weight. The system is more correlated as $1/Z$ deviates more from 1. The electronic correlation become stronger as U increases, and $LaFe_3Si_2$ shows a much stronger correlation than $LaRu_3Si_2$, as expected. The most correlated orbital is $d_{x^2-y^2}$ which contributes to the flat bands near the Fermi level. Therefore, these results indicate that strong electronic correlation would stabilize a perfect Kagome lattice consisting of transition metal ions in the system of LaX_3Si_2 (X = Ru, Fe).

Fig. 2a and b also show that increasing the lattice parameter ratio c/a, i.e., increasing the distance between the Ru_3 Kagome layer and $LaSi_2$ layer, tends to increase x and distort the Kagome plane. Thus, a larger Hubbard U is required to stabilize a perfect Kagome lattice at a larger ratio of c/a.

Fig. 3a and d show the local magnetic susceptibilities $\chi_{\mathrm{loc}}(T)$ calculated by LDA+DMFT for different U. For $LaRu_3Si_2$, $\chi_{\mathrm{loc}}(T)$ shows Pauli paramagnetism behavior at $U = 3$ eV, while it shows a Curie-Weiss-like behavior at $U = 5$ eV. In between, $\chi_{\mathrm{loc}}(T)$ slightly increases with decreasing temperature, which is consistent with that measured by experiment (see Fig. 7 in Ref. [29]). Based on this, we infer that the actual Hubbard U for $LaRu_3Si_2$ is approximately 4 eV. At this U value, $LaRu_3Si_2$ is thus found to be on the verge of crystallizing into a perfect Kagome structure, according to the relaxation results at the experimental lattice parameters shown as the orange curves in Fig. 2a, b. At $U = 4$ eV, the mass-enhancement of the most correlated orbital $d_{x^2-y^2}$ is

DOI: 10.52396/JUSTC-2022-0182
JUSTC, **2023**, 53(7): 0702

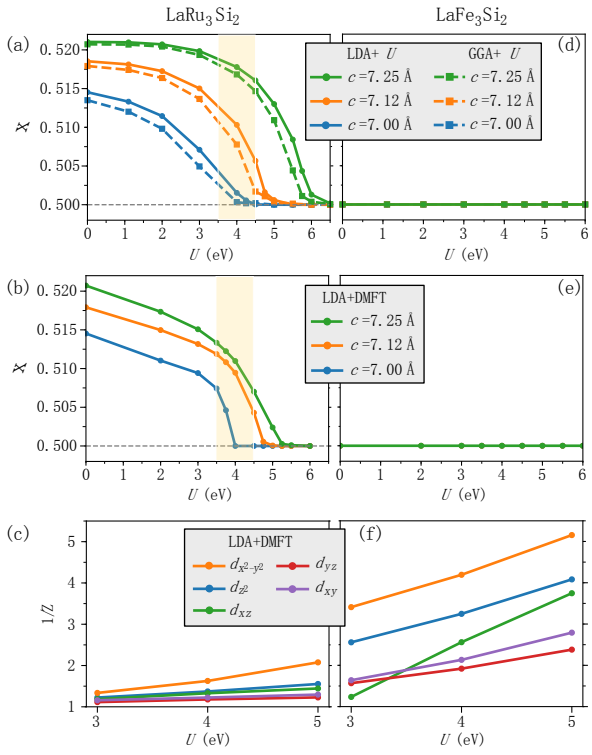

Fig. 2. Electronic correlation effects on stabilizing a perfect Kagome lattice. (a), (d) Fractional coordinates x of Ru (Fe) relaxed by LDA+U and GGA+U as functions of Hubbard U, for different lattice parameter ratio c/a with the fixed crystal volume of experiment. c = 7.12 Å is the experimental value. x = 0.5 for a perfect Kagome lattice. (b), (e) x relaxed by LDA+DMFT as functions of U. The yellow area mark that $LaRu_3Si_2$ is on the verge of becoming a perfect Kagome lattice. (c), (f) LDA+DMFT calculated mass-enhancement of Ru-4d (Fe-3d) orbitals due to electronic correlations, as functions of U. (a)–(c) for $LaRu_3Si_2$ and (d)–(f) for $LaFe_3Si_2$.

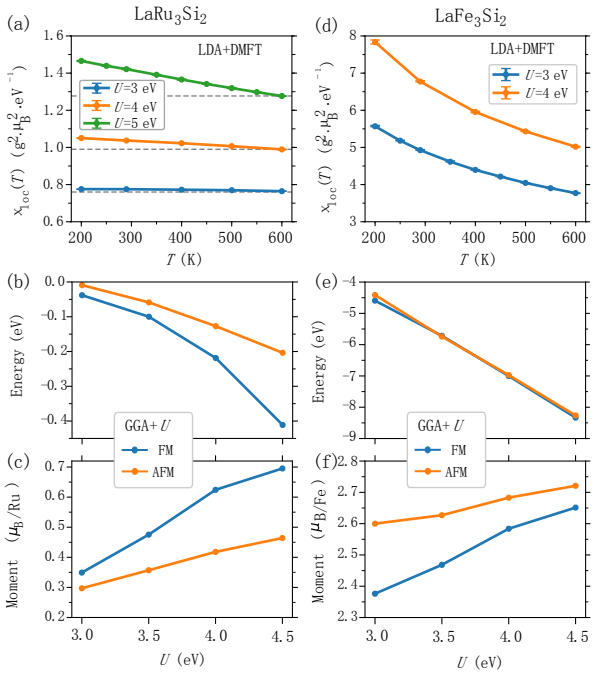

Fig. 3. Electronic correlation induced magnetism. (a), (d) Local magnetic susceptibilities calculated by LDA+DMFT as functions of temperate T for different U values. (b), (e) The energies (per unit cell) of FM and AFM orders with respect to the non-magnetic state as functions of U, calculated by GGA+U. (c), (f) Ordered magnetic moment in the FM and AFM states. (a)–(c) for $LaRu_3Si_2$, the crystal structures relaxed at the corresponding U are used. (d)–(f) for $LaFe_3Si_2$. The experimental lattice parameters, a = 5.676 Å and c = 7.12 Å, are used for both compounds.

approximately 1.63 (Fig. 2c). This indicates a moderate electronic correlation in $LaRu_3Si_2$, consistent with a slightly large Wilson ratio R = 2.88 (R = 1 for non-interacting electron gas) and an NFL contribution to the electronic specific heat, found by the transport experiment[29]. In contrast, $\chi_{loc}(T)$ shows a well-defined Curie-Weiss behavior for $LaFe_3Si_2$, indicating a much stronger electronic correlation and magnetism.

Fig. 3b and e show the energies of the FM and AFM orders with respect to the non-magnetic phase calculated by GGA+U, and Fig. 3c and f show the corresponding ordered magnetic moments. $LaFe_3Si_2$ has very low energies in magnetic states compared to its non-magnetic state and large ordered magnetic moments, suggesting that it tends to order as the temperature decreases. Its FM and AFM states are very close in energy, indicating comparable inter-layer FM and AFM couplings. $LaRu_3Si_2$ shows much weaker magnetism than $LaFe_3Si_2$, but the FM and AFM states are still energetically stable at the static mean-field level. Its FM state has significantly lower energy than the AFM state. Although no magnetic orders have been observed experimentally in $LaRu_3Si_2$, the stable FM state found by the GGA+U calculation suggests that substantial FM fluctuations may exist in $LaRu_3Si_2$. Such FM fluctuations should be attributed to the flat bands near the Fermi level, derived from the Kagome lattice.

Fig. 4 shows the LDA and LDA+DMFT calculated band structures and density of states (DOS) at U = 4 eV and J_H = 0.782 eV in the paramagnetic states. Extremely flat bands with $d_{x^2-y^2}$ characteristics clearly exist near the Fermi level in $LaFe_3Si_2$. However, such bands in $LaRu_3Si_2$ are not as flat as those in $LaFe_3Si_2$. By comparing the band structures between the distorted and perfect Kagome lattices of $LaRu_3Si_2$, we found that the magnitude of distortion of the Kagome lattice has small effects on the flat bands in $LaRu_3Si_2$. Actually, this is mainly caused by the more extended 4d orbitals that will induce non-vanishing hoppings among distant Kagome lattice sites and result in imperfect destructive interference of hoppings. In $LaRu_3Si_2$, the flat bands induce substantial FM fluctuations, as shown in Fig. 3b.

4 Conclusions

To summarize, by taking the Kagome system LaX_3Si_2 (X=Ru, Fe) as an example, we have demonstrated that strong electronic correlations could play important roles in stabilizing a perfect Kagome plane. We show that $LaRu_3Si_2$ is on the verge of becoming a perfect Kagome lattice and it thus exhibits moderate electronic correlation and substantial ferromagnetic fluctuations. A previous study has shown that the electron-phonon couplings alone are not nearly enough to account for a superconducting T_c of 7.8 K in $LaRu_3Si_2$[30]. The electronic correlations and ferromagnetic fluctuations found in our study

DOI: 10.52396/JUSTC-2022-0182
JUSTC, **2023**, 53(7): 0702

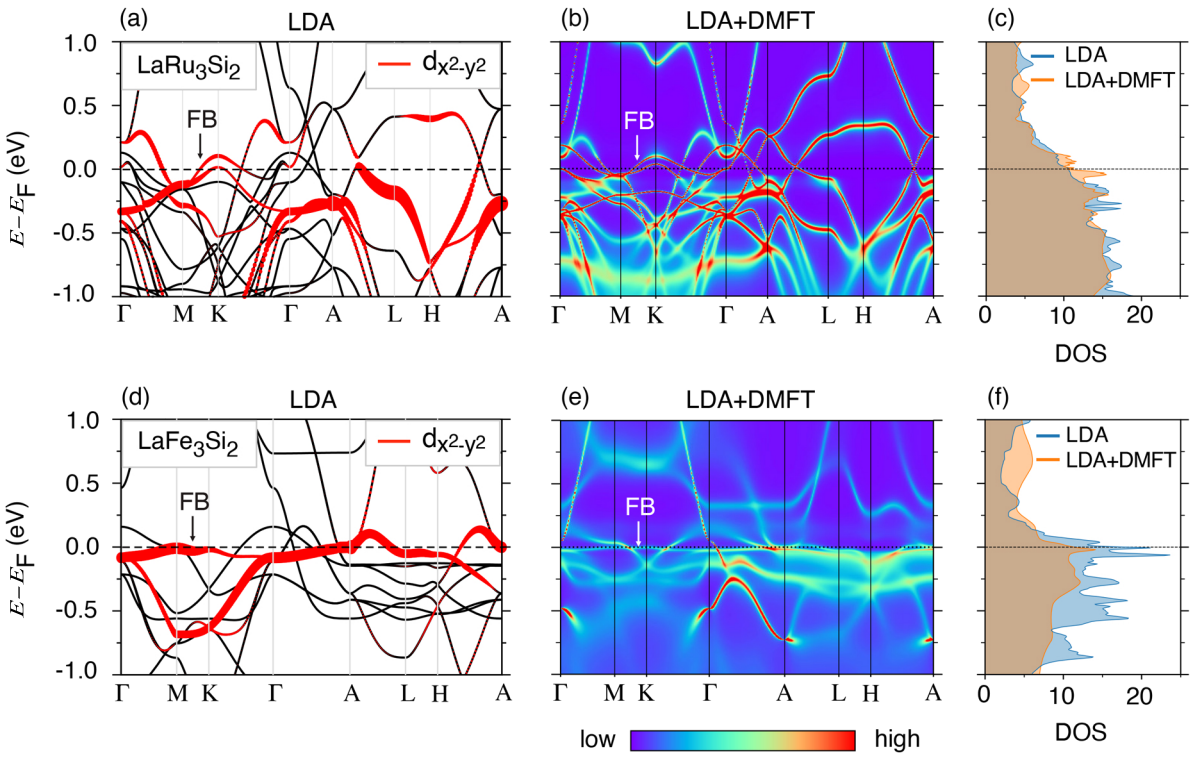

Fig. 4. Flat band near Fermi level. (a), (d) LDA calculated band structures. The flat bands (FB) with $d_{x^2-y^2}$ character are shown in red. (b), (e) LDA+DMFT calculated spectrum function $A(k,\omega)$ at $U = 4$ eV, $J_H = 0.782$ eV, and $T = 290$ K. (c), (f) The corresponding density of states. (a)–(c) for $LaRu_3Si_2$, the crystal structure relaxed by LDA+DMFT at $U = 4$ eV, $J_H = 0.782$ eV is used. (d)–(f) for $LaFe_3Si_2$. The experimental lattice parameters, $a = 5.676$ Å and $c = 7.12$ Å, are used for both compounds.

may play significant roles in enhancing T_c of $LaRu_3Si_2$, which is worthy of further study.

As shown in the Fig. S3 in the supporting information, the only obvious difference in the simulated powder diffraction pattern of $LaRu_3Si_2$ between the space groups $P6_3/mcm$ and $P6_3/m$ is an additional reflection at (1 0 1) for $P6_3/m$. However, its intensity is very weak compared to the main peak such that it is very difficult to resolve experimentally. Further high-resolution crystal structure refinement with high-quality samples is required to determine whether $LaRu_3Si_2$ crystallizes into the space group $P6_3/mcm$. Our result thus provides a reference for the crystal structure refinement of $LaRu_3Si_2$.

Supporting information

The supporting information for this article can be found online at https://doi.org/10.52396/JUSTC-2022-0182. The supporting information includes values of U and J_H, magnetic configurations, results of crystal relaxation of $LaRu_3Si_2$ by GGA+SOC+U, and simulated XRD pattern of $LaRu_3Si_2$ for space group $P6_3/mcm$ and $P6_3/m$. There are three figures and one table in the supporting information.

Acknowledgements

This work was supported by the USTC Research Funds of the Double First-Class Initiative (YD2340002005). All the calculations presented in this work were preformed on TianHe-1A, the National Supercomputer Center in Tianjin, China.

Conflict of interest

The author declares that he has no conflict of interest.

Biography

Yilin Wang is currently a Research Professor at School of Emerging Technology, University of Science and Technology of China. He received his Ph.D. degree from Institute of Physics, CAS in 2016. His research mainly focuses on first-principle calculations of strongly correlated electronic materials using DFT plus dynamical mean-filed theory.

References

[1] Syôzi I. Statistics of Kagomé lattice. *Progress of Theoretical Physics,* **1951**, *6* (3): 306–308.
[2] Mielke A. Ferromagnetic ground states for the Hubbard model on line graphs. *Journal of Physics A: Mathematical and General,* **1991**, *24*: L73.
[3] Tasaki H. Ferromagnetism in the Hubbard models with degenerate single-electron ground states. *Physical Review Letters,* **1992**, *69*: 1608.
[4] Sachdev S. Kagomé- and triangular-lattice Heisenberg antiferromagnets: Ordering from quantum fluctuations and quantum-disordered ground states with unconfined bosonic spinons. *Physical Review B,* **1992**, *45*: 12377.
[5] Tang E, Mei J W, Wen X G. High-temperature fractional quantum Hall states. *Physical Review Letters,* **2011**, *106*: 236802.
[6] Cao Y, Fatemi V, Fang S, et al. Unconventional superconductivity in magic-angle graphene superlattices. *Nature,* **2018**, *556*: 43–50.
[7] Balents L, Dean C R, Efetov D K, et al. Superconductivity and strong correlations in moiré flat bands. *Nature Physics,* **2020**, *16*: 725–733.

DOI: 10.52396/JUSTC-2022-0182
JUSTC, **2023**, 53(7): 0702

[8] Aoki H. Theoretical possibilities for flat band superconductivity. *Journal of Superconductivity and Novel Magnetism,* **2020**, *33*: 2341–2346.
[9] Heikkilä T T, Volovik G E. Flat bands as a route to high-temperature superconductivity in graphite. In: Esquinazi P, editor. Basic Physics of Functionalized Graphite. Cham: Springer International Publishing, **2016**: 123–143.
[10] Jiang K, Wu T, Yin J X, et al. Kagome superconductors AV_3Sb_5 (A = K, Rb, Cs). *National Science Review,* **2022**, *10* (2): nwac199.
[11] Nie L, Sun K, Ma W, et al. Charge-density-wave-driven electronic nematicity in a kagome superconductor. *Nature,* **2022**, *604*: 59–64.
[12] Jiang Y X, Yin J X, Denner M M, et al. Unconventional chiral charge order in kagome superconductor KV_3Sb_5. *Nature Materials,* **2021**, *20*: 1353–1357.
[13] Teng X, Chen L, Ye F, et al. Discovery of charge density wave in a kagome lattice antiferromagnet. *Nature,* **2022**, *609*: 490–495.
[14] Kang M, Ye L, Fang S, et al. Dirac fermions and flat bands in the ideal kagome metal FeSn. *Nature Materials,* **2020**, *19*: 163–169.
[15] Lin Z, Wang C, Wang P, et al. Dirac fermions in antiferromagnetic FeSn kagome lattices with combined space inversion and time-reversal symmetry. *Physical Review B,* **2020**, *102*: 155103.
[16] Huang L, Lu H. Signatures of hundness in kagome metals. *Physical Review B,* **2020**, *102*: 125130.
[17] Ye L, Kang M, Liu J, et al. Massive Dirac fermions in a ferromagnetic kagome metal. *Nature,* **2018**, *555*: 638–642.
[18] Lin Z, Choi J H, Zhang Q, et al. Flatbands and emergent ferromagnetic ordering in Fe_3Sn_2 kagome lattices. *Physical Review Letters,* **2018**, *121*: 096401.
[19] Yin J X, Zhang S S, Li H, et al. Giant and anisotropic many-body spin-orbit tunability in a strongly correlated kagome magnet. *Nature,* **2018**, *562*: 91–95.
[20] Kang M, Fang S, Ye L, et al. Topological flat bands in frustrated kagome lattice CoSn. *Nature Communications,* **2020**, *11*: 4004.
[21] Liu Z, Li M, Wang Q, et al. Orbital-selective Dirac fermions and extremely flat bands in frustrated kagome-lattice metal CoSn. *Nature Communications,* **2020**, *11*: 4002.
[22] Yin J X, Shumiya N, Mardanya S, et al. Fermion-boson many-body interplay in a frustrated kagome paramagnet. *Nature Communications,* **2020**, *11*: 4003.
[23] Meier W R, Du M H, Okamoto S, et al. Flat bands in the CoSn-type compounds. *Physical Review B,* **2020**, *102*: 075148.
[24] Huang H, Zheng L, Lin Z, et al. Flat-band-induced anomalous anisotropic charge transport and orbital magnetism in kagome metal CoSn. *Physical Review Letters,* **2022**, *128*: 096601.
[25] Yin J X, Ma W, Cochran T A, et al. Quantum-limit Chern topological magnetism in $TbMn_6Sn_6$. *Nature,* **2020**, *583*: 533–536.
[26] Yang T Y, Wan Q, Song J P, et al. Fermi-level flat band in a kagome magnet. *Quantum Frontiers,* **2022**, *1*: 14.
[27] Vandenberg J M, Barz H. The crystal structure of a new ternary silicide in the system rare-earth-ruthenium-silicon. *Materials Research Bulletin,* **1980**, *15* (10): 1493–1498.
[28] Li B, Li S, Wen H H. Chemical doping effect in the $LaRu_3Si_2$ superconductor with a kagome lattice. *Physical Review B,* **2016**, *94*: 094523.
[29] Li S, Zeng B, Wan X, et al. Anomalous properties in the normal and superconducting states of $LaRu_3Si_2$. *Physical Review B,* **2011**, *84*: 214527.
[30] Mielke C, Qin Y, Yin J X, et al. Nodeless kagome superconductivity in $LaRu_3Si_2$. *Physical Review Materials,* **2021**, *5*: 034803.
[31] Gong C, Tian S, Tu Z, et al. Superconductivity in kagome metal YRu_3Si_2 with strong electron correlations. *Chinese Physics Letters,* **2022**, *39*: 087401.
[32] Anisimov V I, Zaanen J, Andersen O K. Band theory and Mott insulators: Hubbard *U* instead of Stoner *I*. *Physical Review B,* **1991**, *44*: 943.
[33] Georges A, Kotliar G, Krauth W, et al. Dynamical mean-field theory of strongly correlated fermion systems and the limit of infinite dimensions. *Reviews of Modern Physics,* **1996**, *68*: 13.
[34] Lichtenstein A I, Katsnelson M I, Kotliar G. Finite-temperature magnetism of transition metals: An *ab initio* dynamical mean-field theory. *Physical Review Letters,* **2001**, *87*: 067205.
[35] Kotliar G, Savrasov S Y, Haule K, et al. Electronic structure calculations with dynamical mean-field theory. *Reviews of Modern Physics,* **2006**, *78*: 865.
[36] Momma K, Izumi F. *VESTA*: A three-dimensional visualization system for electronic and structural analysis. *Journal of Applied Crystallography,* **2008**, *41*: 653–658.
[37] Kresse G, Furthmüller J. Efficient iterative schemes for *ab initio* total-energy calculations using a plane-wave basis set. *Physical Review B,* **1996**, *54*: 11169.
[38] Blöchl P E. Projector augmented-wave method. *Physical Review B,* **1994**, *50*: 17953.
[39] Perdew J P, Burke K, Ernzerhof M. Generalized gradient approximation made simple. *Europace,* **1996**, *77*: 3865.
[40] Liechtenstein A I, Anisimov V I, Zaanen J. Density-functional theory and strong interactions: Orbital ordering in Mott-Hubbard insulators. *Physical Review B,* **1995**, *52*: R5467.
[41] Haule K, Yee C H, Kim K. Dynamical mean-field theory within the full-potential methods: Electronic structure of $CeIrIn_5$, $CeCoIn_5$, and $CeRhIn_5$. *Physical Review B,* **2010**, *81*: 195107.
[42] Haule K, Birol T. Free energy from stationary implementation of the DFT+DMFT functional. *Physical Review Letters,* **2015**, *115*: 256402.
[43] Blaha P, Schwarz K, Tran F, et al. WIEN2k: An APW+lo program for calculating the properties of solids. *The Journal of Chemical Physics,* **2020**, *152* (7): 074101.
[44] Gull E, Millis A J, Lichtenstein A I, et al. Continuous-time Monte Carlo methods for quantum impurity models. *Reviews of Modern Physics,* **2011**, *83*: 349.
[45] Haule K. Exact double counting in combining the dynamical mean field theory and the density functional theory. *Physical Review Letters,* **2015**, *115*: 196403.
[46] Haule K, Pascut G L. Forces for structural optimizations in correlated materials within a DFT+embedded DMFT functional approach. *Physical Review B,* **2016**, *94*: 195146.
[47] Haule K. DFT+embedded DMFT Functional. [2022-10-11] http://hauleweb.rutgers.edu/tutorials/index.html.

DOI: 10.52396/JUSTC-2022-0182
JUSTC, **2023**, 53(7): 0702